Accepted Manuscript

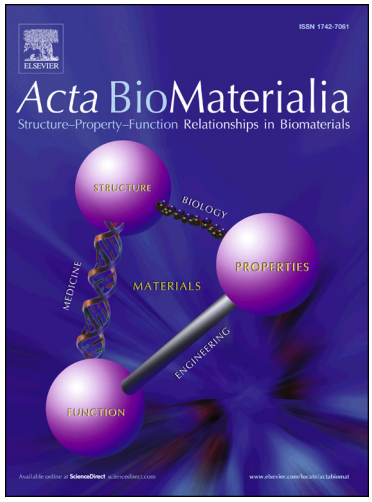

Full length article

Rate-dependency of the mechanical behaviour of semilunar heart valves under biaxial deformation

Afshin Anssari-Benam, Yuan-Tsan Tseng, Gerhard A. Holzapfel, Andrea Bucchi

PII: S1742-7061(19)30112-6
DOI: https://doi.org/10.1016/j.actbio.2019.02.008
Reference: ACTBIO 5937

To appear in: *Acta Biomaterialia*

Received Date: 25 September 2018
Revised Date: 25 January 2019
Accepted Date: 8 February 2019

Please cite this article as: Anssari-Benam, A., Tseng, Y-T., Holzapfel, G.A., Bucchi, A., Rate-dependency of the mechanical behaviour of semilunar heart valves under biaxial deformation, *Acta Biomaterialia* (2019), doi: https://doi.org/10.1016/j.actbio.2019.02.008

Rate-dependency of the mechanical behaviour of semilunar heart valves under biaxial deformation

Afshin Anssari-Benam[1,*], Yuan-Tsan Tseng[2], Gerhard A. Holzapfel[3,4] and Andrea Bucchi[1]

[1] Cardiovascular Engineering Research Laboratory (CERL), School of Mechanical and Design Engineering, University of Portsmouth, Anglesea Road, Portsmouth PO1 3DJ, United Kingdom

[2] National Heart and Lung Institute, Heart Science Centre, Imperial College London, Middlesex, United Kingdom

[3] Graz University of Technology, Institute of Biomechanics. Graz, Austria

[4] Norwegian University of Science and Technology (NTNU), Faculty of Engineering Science and Technology, Trondheim, Norway

* Address for correspondence:
Afshin Anssari-Benam,
Cardiovascular Engineering Research Laboratory (CERL),
School of Mechanical and Design Engineering,
University of Portsmouth,
Anglesea Road,
Portsmouth PO1 3DJ
United Kingdom

Tel: +44 (0)23 9284 2187
Fax: +44 (0)23 9284 2351
E-mail: afshin.anssari-benam@port.ac.uk

Abstract

This paper presents an experimental investigation and evidence of rate-dependency in the planar mechanical behaviour of semilunar heart valves. Samples of porcine aortic and pulmonary valves were subjected to biaxial deformations across 1000-fold stretch rate, ranging from $\dot{\lambda} = 0.001$ to $1s^{-1}$. The experimental campaign encompassed protocols covering (i) tests on samples without preconditioning, (ii) preconditioning immediately followed by tensile tests; and (iii) tensile tests at different rates performed on the same preconditioned specimen. Our results indicate that under all employed loading protocols, heart valve samples exhibit a marked rate-dependency in their deformation behaviour. This rate-dependency is reflected in stress-stretch curves and the calculated ensuing gradients, where samples typically show stiffening with increased rate. These results underpin one conclusive outcome: the in-plane mechanical behaviour of semilunar valves is rate-dependent ($p < 0.055$ for Cauchy stress levels $\geq$50 kPa). This outcome implies that the rate of deformation for characterising the mechanical behaviour of semilunar heart valves may not be chosen arbitrarily low, and models that incorporate rate-effects may be more appropriate for better capturing the mechanical behaviour of heart valves.

Keywords: aortic valve, pulmonary valve, rate-dependency, biaxial deformation, mechanical behaviour

Rate-dependency of the mechanical behaviour of semilunar heart valves under biaxial deformation

Introduction

Viscoelastic attributes of the mechanical behaviour of heart valves, such as exhibiting stress relaxation [1-5] and creep [1,2] under different loading boundary conditions have been well documented. An integral manifestation of viscoelasticity is also the rate-dependency in the mechanical behaviour of subject tissues. However, and perhaps surprisingly, the in-plane mechanical behaviour of heart valves has been frequently characterised within the framework of (hyper)elasticity. Therefore, the rate dependency of the in-plane mechanical behaviour of heart valves, and in particular semilunar valves which include the aortic and pulmonary valves, has been discounted. Discounting the rate effects has perpetuated in the literature despite the lack of existence of comprehensive set of data, to date, to conclude rate-independency in the mechanical behaviour of these valves. Indeed, contrary to this rate-independency notion, recent studies have provided primary evidence on the rate-dependency of the mechanical behaviour of the aortic valve (AV) under uniaxial and biaxial tensile deformations [6-8]. These findings motivate further investigation of the rate-dependent characteristics of the mechanical behaviour of semilunar valves, and development of appropriate platforms to accommodate these characteristics.

In the particular case of the AV, accounting for the rate effects on the mechanical behaviour of the native tissue may prove to be of critical importance. The *in vivo* strain rates endured by the valve in its physiological function are thought to be approximately $440\%s^{-1}$ and $1240\%s^{-1}$ in the (principal) circumferential and radial loading directions, corresponding to stretch rates of $\dot{\lambda} = 4.4s^{-1}$ and $\dot{\lambda} = 12.4s^{-1}$, respectively [9]. Based on direct *in vivo* measurements [10], extension rates as high as 50 to 150mm/s are required *in vitro* under which the physiological rate may be replicated [11,12]. From the experimental setup point of view, it is technically challenging to replicate these loading conditions *in vitro*. Resorting to lower rates to gather experimental data in order to calibrate/validate hyperelastic models may underestimate the true deformation behaviour of the tissue *in vivo*, if the rate-effects are not properly understood or accounted for.

It may be argued that employing preconditioning protocols could help eliminating the rate effects, as preconditioned specimens are generally considered rate-insensitive, perhaps following the seminal works of Fung [13,14]. We put this notion to the test for semilunar heart valves in this paper, using porcine AV and pulmonary valve (PV) specimens, tested across a 1000-fold range of deformation rates. When tested across this range, the results indicate a clear rate-dependency in stress-stretch ($\sigma - \lambda$) curves under biaxial deformation both before and after preconditioning. However, even if we accept the premise that preconditioning could abate the rate effects across sufficiently small deformation rates, the fact still remains that the tissue is intrinsically viscoelastic. Therefore, it is incumbent on accurate material characterisation and modelling to account for the viscoelastic features of the valves including the rate-dependency.

In this paper we investigate and present evidence of rate-dependency in the mechanical behaviour of porcine AV and PV tissues under biaxial deformation. Tests are performed on samples with no preconditioning as well as on samples immediately after preconditioning, with the addition of subjecting same samples to both fast and slow deformations, to conclusively document the existence of rate effect in the planar mechanical behaviour of semilunar valves. We confer our analysis on the implications of these results for appropriate characterisation of the mechanical behaviour of heart valves and development of new modelling criteria to account for the observed rate-dependency.

Materials and methods

Here we report the results for samples acquired from a total of 10 porcine hearts, obtained from mature animals ranging from 24 to 36 months old, within 2h of slaughter from a local abattoir. The three AV and PV leaflets were dissected from the hearts and maintained in Dulbecco's Modified Eagle's Medium (DMEM, Sigma, Poole, UK) at room temperature (20°C). From each leaflet, a 12 x 12mm square sample was excised from the central region (schematically shown in Figure 1). The square samples were then subjected to biaxial loading protocols. For tests with slow deformation rate, sample hydration was maintained by sparse spraying over the test period. Fast deformation rate tests had a typical duration of 0.2 to 0.35s, with no additional hydration provision.

Experimental setup and data acquisition

After excision, the sample thickness was measured using a non-contact confocal sensor (Micro-Epsilon (με®) confocalDT - IFC2451), customised for measurement of the thickness of our samples. The average (±SD) measured thickness for AV and PV specimens used in this study reported values of 0.86 ± 0.18mm and 0.75 ± 0.20mm, respectively. The samples were then mounted on a TA Instruments ElectroForce® planar biaxial TestBench device using BioRake (CellScale®) tines as part of a custom-designed sample mounting mechanism. An image of the experimental setup is shown in Figure 2. Five ink-marker points were printed on the centre of the specimens as fiducials for measuring and calculating the principal stretches λ, and their centroids were tracked over the period of deformation using an in-house video camera, recording at 30-240 frames per second depending on the stretch rate at each test. The recorded frames were then analysed using a custom-developed code in MATLAB®, devised based on the procedure outlined by Humphrey (2002) [15]. Typical quadrilaterals reconstructed from the trajectory of the markers at each frame using this method are shown in Figure 2d. For more details the interested reader is referred to our previous study [8].

Equi-biaxial rate tests on samples with no preconditioning

Three Cauchy stress-stretch ($\sigma - \lambda$) curves for AV samples subjected to applied equi-biaxial deformation stretch rates of $\dot{\lambda} = 0.001$ and $1s^{-1}$ without preconditioning were reconstructed from those reported in our previous study [8], and additional three fresh samples were tested at those rates (without preconditioning) to provide a total of six AV specimens. For PV specimens, however, six fresh samples were subjected to equi-biaxial deformation rate tests at $\dot{\lambda} = 0.001$ to $1s^{-1}$ each. A tare load of 0.01N was applied to all samples in both loading directions to ensure a consistent starting position.

Equi-biaxial rate tests on preconditioned samples

For this group of tests, a preconditioning protocol was applied on specimens, immediately followed by the equi-biaxial deformation. For AV specimens, the preconditioning protocol consisted of 25 loading-unloading cycles at 0.5Hz, to the amplitude of 0.5N. A similar protocol was adopted for PV samples, except for a magnitude of 0.3N. After preconditioning,

samples were immediately subjected to deformation tests. Six AV and PV samples were used for equi-biaxial deformation rate tests to failure at $\dot{\lambda}$ =0.001 and 1s^{-1} each. Similar to the other tests, samples were subjected to a tare load of 0.01N prior to the start of the deformation.

Equi-biaxial rate tests at different stretch rates on same samples

Only AV samples were subjected to this test. After preconditioning, each specimen was subjected to two equi-biaxial rate tests ($\dot{\lambda}$ =0.001 and 1s^{-1}), first loaded at $\dot{\lambda}$ =1s^{-1} and then at $\dot{\lambda}$ =0.001s^{-1}. Tests were carried out under displacement control, up to 0.75 and 1mm displacements, separately. Over all twelve samples were used for this group of tests.

Statistical analysis

To ascertain statistical significance in the rate-dependency of the in-plane mechanical behaviour of the specimens, the gradient of the obtained $\sigma - \lambda$ curves was used as a comparing measure. This gradient, i.e. $\frac{\Delta\sigma}{\Delta\lambda}$, was calculated numerically at σ = 10, 50, 100 and 200 kPa, from curves obtained under both fast and slow deformation rates for each of the tested six AV and PV samples. A Kolmogorov-Smirnov test using GraphPad Prism® was performed on each group first to check for the normality of the distribution of the $\frac{\Delta\sigma}{\Delta\lambda}$ values. None of the paired groups, at $\dot{\lambda}$ =0.001s^{-1} and $\dot{\lambda}$ =1s^{-1}, returned a normal distribution. A Mann-Whitney test was thus performed to establish the *p* values between each gradient group, with statistical significance set at p<0.05.

Results

We start by presenting the results obtained from samples with no preconditioning. The experimental data were filtered using a Savitzky-Golay filter and the ensuing Cauchy stress-stretch ($\sigma - \lambda$) curves are presented in Figure 3. Plots contain curves for both AV and PV samples, tested at $\dot{\lambda}$ =1s^{-1} (Figure 3a) and $\dot{\lambda}$ =0.001s^{-1} (Figure 3b). From these filtered datasets, averaged data were calculated by averaging the stretch and stress values at each time step over the six repeats. The ensuing curves in the circumferential (blue) and radial (red)

directions are presented in Figure 3c. The bars represent the standard deviation at the designated points on the curves.

Using the same sequence and graphics, $\sigma - \lambda$ curves obtained from deformation tests immediately after preconditioning the AV and PV samples are shown in Figure 4. Similar to the results for samples without preconditioning, averaged data were constructed and are shown in Figure 4c.

It must be noted that the designated rates of deformation, $\dot{\lambda}$, above are the applied rates by the gripping mechanism onto the specimen. True deformation rates endured at the central region of the specimens covered by the fiducials were calculated using the movements of the markers *a posteriori*. The average deformation rates in the principal loading directions for both AV and PV specimens are presented in Table 1. Note that in both tissue samples, the rate of deformation at the central region of specimens is lower than the applied rate, but typically possessing higher values in the radial direction.

From these curves, values of the gradient $\frac{\Delta\sigma}{\Delta\lambda}$ were calculated numerically at the designated stress levels (σ = 10, 50, 100 and 200 kPa) and are presented in Tables 2 and 3 for AV and PV specimens, respectively, together with the p values comparing the gradients of fast and slow curves.

The final set of results relates to the tests performed at $\dot{\lambda}$ =0.001 and 1s^{-1} rates on the same specimen. Two representative (filtered) $\sigma - \lambda$ curves obtained from tested AV samples are shown in Figure 5, each separately stretched up to 1mm (Figure 5a) and 0.75mm (Figure 5b).

Discussion

The aim of this study was to provide, to our knowledge, the first comprehensive evidence that the planar mechanical behaviour of semilunar heart valves is rate-dependent. Results from samples with no preconditioning together with the results from preconditioned samples immediately followed by deformation tests conclusively underline the rate-dependency of the mechanical behaviour of AV and PV samples under biaxial deformation, as presented in

Figures 3 and 4. The averaged data summarise this feature graphically, showing typically a stiffening behaviour with the increase in the stretch rate.

Our preconditioning procedure consisted of a load-controlled protocol, cyclically loading the samples to 0.5N and 0.3N for AV and PV specimens, respectively, at a frequency of 0.5Hz. Deformation tests immediately followed the preconditioning. To our understanding, there is no consensus in the literature regarding the rest time, the time between the end of preconditioning and the start of the deformation test. Studies in soft tissue biomechanics employ a range of resting periods, varying from 30mins [16] to 10mins [17], or even more specialised procedures such as 5mins of stress-relaxation [11]. In this study we have employed two extreme opposites, from no preconditioning at all to tests immediately after preconditioning. Rate-dependency in the $\sigma - \lambda$ curves is clearly visible in both extremities, and, therefore, any resting period that may be employed in testing the valvular tissues will fall within these extremities and will not eliminate the rate-effects on $\sigma - \lambda$ curves.

We also note that the rate effects in the $\sigma - \lambda$ curves obtained from preconditioned samples is somewhat less pronounced than that of samples without preconditioning. Preconditioning therefore down-regulated the rate effect; however, it is evident that it does not completely eliminate it, if samples are tested across a sufficiently large span of deformation rates. We further note that we have not considered any shearing effects in our experiments. To the best of practical possibility, samples were mounted within the testing device such that the principal axes of the material coincided with the loading axes. As the typical quadrilaterals in Figure 2 show, shear deformation was deemed negligible and was not taken into account in our analyses. The specimen mounting procedure used in this study is similar to those used for other cardiac tissues, where negligible amount of shearing effects has been documented [18].

At this point, an argument can be made that the average curves, e.g. the curves shown in Figures 3c and 4c, are mathematical averages and therefore the observed rate effects may not represent a real material behaviour. In order to eliminate this doubt, we took two additional approaches. First approach was to use the $\frac{\Delta\sigma}{\Delta\lambda}$ gradient, obtained numerically from the $\sigma - \lambda$ curves of all samples, as a measure of rate-dependency. Comparing the gradient(s) between the curves obtained at fast and slow rates for all samples and ascertaining a statistically significant difference provides additional support to the observed rate-dependent behaviour

through the average curves. Accordingly, the gradients were calculated at σ = 10, 50, 100 and 200 kPa. This range was chosen to allow an assessment of the evolution of differences in the gradients between the fast and slow $\sigma - \lambda$ curves, from the initial stages of the curves (very low stresses) to near physiological levels. Tables 2 and 3 present the numerical values for all AV and PV specimens, respectively, along with the calculated *p* values.

As the tables indicate, not all samples show a statistically significant difference in the gradient of their $\sigma - \lambda$ curves at low stress levels. However, there is a significant statistical difference between the gradients of all samples at $\sigma \geq$50 kPa. Therefore, our statistical analysis reinforces the point that the averaged data illustrate: $\sigma - \lambda$ curves of the specimens are rate-dependent, typically showing a stiffening behaviour with the increase in rate.

The second approach we took was to perform tests at $\dot{\lambda}$ =0.001s^{-1} and $\dot{\lambda}$ =1s^{-1} on the same AV (preconditioned) specimens, and record the deformation curves (see 'Methods' section). In the first set of tests, we stretched the samples in both directions to 1mm, initially at $\dot{\lambda}$ =1s^{-1}, then unloaded the sample and stretched it again to 1mm but this time at $\dot{\lambda}$ =0.001s^{-1}. Representative $\sigma - \lambda$ curves are shown in Figure 5a. Graphs indicate a clear rate-dependent response.

To eliminate the possibility that the samples, though not visible at the macrostructure, may have been damaged during the first test at the microstructure, we repeated the tests with new samples for 0.75mm of displacement, to avoid getting close to or exceeding the 'elastic' limit of the tissue. The ensuing representative $\sigma - \lambda$ curves are shown in Figure 5b. Similar to the previous case, rate-dependency is evident. Noting that the induced Cauchy stress in both cases is way below the physiological stress (240 kPa) of the functioning valve [5], we are confident that the curves do not embody any structural damage artefact. We do not present the results for the PV samples, as due to the much softer nature of the PV tissue, we were not able to ascertain a meaningful level of force (stress) for comparison, when we loaded the samples up to 0.75mm or 1mm, particularly in the radial direction. With the given sensitivity of the load cells, a larger displacement range was required for a meaningful comparison. Performing the fast rate tests on PV samples at displacements of 2mm and above, we found that the samples were damaged at the gripping sites, and therefore the results from second test did not meaningfully represent the true behaviour of the sample. Subject to successful tests,

we have no reason to believe that PV samples would behave differently to AV samples, as PV $\sigma - \lambda$ curves under equi-biaxial rate deformations at $\dot{\lambda} = 1$ and $0.001 s^{-1}$, and the gradients $\frac{\Delta\sigma}{\Delta\lambda}$ of the curves, clearly demonstrate rate-dependency trends similar to AV samples (see Figures 3, 4 and Table 3).

In general, as the averaged data in Figures 3 and 4 and the *p* values in Tables 2 and 3 indicate, rate-dependency in the in-plane mechanical behaviour of the PV appears to be less pronounced than of the AV. Representative images of the macrostructure, histology and the Maximum Projection Intensity (MPI) of the collagen fibres taken from typical AV and PV specimens, shown in Figure 1, visually demonstrate a less-dense fibre population in the PV tissue compared with the AV. In a recent study, we stipulated that the viscoelastic features of the AV may partly stem from fibre-fibre and fibre-matrix dissipative interactions [2], based on micro- and macro-level experimental observations [2,19]. In this regard, the less-pronounced rate-dependent behaviour of the PV may be attributed to the lower collagen fibre content of the tissue, and is therefore consistent with the expected behaviour.

Implications of these results for a better understanding of the true mechanical behaviour of semilunar valves under physiological function, and accurate modelling of their mechanical behaviour *in vivo* and *in vitro*, may prove significant. First, the results of this study clearly indicate that the experimental mechanical behaviours obtained under quasi-static or even relatively slow deformations may not be an accurate representative of the *in vivo* behaviour of the valves. The indications are that it is necessary to characterise the mechanical behaviour of the tissues at rates as close to the physiological deformation rates as possible, even after preconditioning. Certainly, deformation rates employed in characterising the mechanical behaviour of the valves cannot be arbitrary low. In this regard, it may also prove useful to investigate and establish the existence of a possible rate threshold below which the observed mechanical behaviour would be distinctly different to the physiological behaviour. Second, since this data clearly demonstrates rate-dependency in the mechanical behaviour of the semilunar valves, it is incumbent on mathematical/computational models to accurately represent this feature of valvular tissues. It may therefore be necessary to develop continuum-based models that account for the rate-dependent behaviour of the valves.

Acknowledgment

This work was part of a visiting professorship program funded by the Leverhulme Trust (VP1-2017-001). The authors wish to thank Dr. Padmini Sarathchandra, Heart Science Centre, for her kind assistance with histology and second harmonic generation imaging of the samples.

Disclosure statement

The authors have no conflict of interest to declare.

References

[1] A. Anssari-Benam, D. L. Bader, H. R. C. Screen, Anisotropic time-dependant behaviour of the aortic valve, Journal of the Mechanical Behavior of Biomedical Materials 4 (2011) 1603-1610.

[2] A. Anssari-Benam, H. R. C. Screen, A. Bucchi, Insights into the micromechanics of stress-relaxation and creep behaviours in the aortic valve, Journal of the Mechanical Behavior of Biomedical Materials, Submitted.

[3] S. Huang, H. -Y. Shadow Huang, Biaxial stress relaxation of semilunar heart valve leaflets during simulated collagen catabolism: Effects of collagenase concentration and equibiaxial strain state, Proceedings of the Institution of Mechanical Engineers, Part H: Journal of Engineering in Medicine 229 (2015) 721-731.

[4] J. Liao, L. Yang, J. Grashow, M. S. Sacks, The relation between collagen fibril kinematics and mechanical properties in the mitral valve anterior leaflet, Journal of Biomechanical Engineering 129 (2007) 78-87.

[5] J. A. Stella, J. Liao, M. S. Sacks, Time-dependent biaxial mechanical behavior of the aortic heart valve leaflet, Journal of Biomechanics 40 (2007) 3169-3177.

[6] A. Anssari-Benam, D. L. Bader, H. R. C. Screen, A combined experimental and modelling approach to aortic valve viscoelasticity in tensile deformation, Journal of Materials Science: Materials in Medicine 22 (2011) 253-262.

[7] A. Anssari-Benam, A. Bucchi, H. R. C. Screen, S. L. Evans, A transverse isotropic viscoelastic constitutive model for aortic valve tissue, Royal Society Open Science (2017). doi: 10.1098/rsos.160585.

[8] A. Anssari-Benam, Y.-T. Tseng, and A. Bucchi, A transverse isotropic constitutive model for the aortic valve tissue incorporating rate-dependency and fibre dispersion: application to biaxial deformation, Journal of the Mechanical Behavior of Biomedical Materials 85 (2018) 80-93.

[9] M. S. Sacks, A. P. Yoganathan, Heart valve function: a biomechanical perspective, Philosophical Transactions of the Royal Society B: Biological Sciences 362 (2007) 1369-1391.

[10] M. J. Thubrikar, J. L. Heckman, S. P. Nolan, High speed cine-radiographical study of aortic valve leaflet motion, The Journal of Heart Valve Disease 2 (1993) 653-661.

[11] E. O. Carew, A. Garg, J. E. Barber, I. Vesely, Stress relaxation preconditioning of porcine aortic valves, Annals of Biomedical Engineering 32 (2004) 563-5672.

[12] T. C. Doehring, E. O. Carew, I. Vesely, The effect of strain rate on the viscoelastic response of aortic valve tissue: A direct-fit approach, Annals of Biomedical Engineering 32 (2004) 223-232.

[13] Y. C. Fung, Biomechanics: Mechanical properties of living tissues. 2nd edition, New York: Springer-Verlag, 1993, pp.270.

[14] Y. C. Fung, Structure and stress-strain relationship of soft tissues, American Zoologist 24 (1984) 13-22.

[15] J. D. Humphrey, Cardiovascular solid mechanics: Cells, tissues, and organs. New York: Springer-Verlag, 2002, pp. 172–175.

[16] D. P. Pioletti, L. R. Rakotomanana, J. F. Benvenuti, P. F. Leyvraz, Viscoelastic constitutive law in large deformations: application to human knee ligaments and tendons, Journal of Biomechanics 31 (1998) 753-757.

[17] O. Lokshin, Y. Lanir, Micro and macro rheology of planar tissues, Biomaterials 30 (2009) 3118-3127.

[18] G. Sommer, D. H. Haspinger, M. Andra, M. Sacherer, C. Viertler, P. Regiting, G. A. Holzapfel, Quantification of shear deformations and corresponding stresses in the biaxially tested human myocardium, Annals of Biomedical Engineering 43 (2015) 2334 - 2348.

[19] A. Borghi, S. E. P. New, A. H. Chester, P. M. Taylor, M. H. Yacoub, Time-dependent mechanical properties of aortic valve cusps: Effect of glycosaminoglycan depletion, Acta Biomaterialia 9 (2013) 4645-4652.

Table legends

Table 1 - Corresponding stretch rates in the central region of the specimens in both loading directions.

Table 2 - Numerical values of the gradient $\frac{\Delta\sigma}{\Delta\lambda}$ calculated at the designated stress levels for all tested AV specimens. Statistical significance (p) values were established using a Mann-Whitney test.

Table 3 - Numerical values of the gradient $\frac{\Delta\sigma}{\Delta\lambda}$ calculated at the designated stress levels for all tested PV specimens. Statistical significance (p) values were established using a Mann-Whitney test.

Table 1

	$\dot{\lambda}$ [s^{-1}] at the central region			
	AV specimens		PV specimens	
Applied $\dot{\lambda}$ [s^{-1}]	Circumferential	Radial	Circumferential	Radial
0.001	0.0005 ± 0.0001	0.0013 ± 0.0009	0.0003 ± 0.0001	0.0012 ± 0.0002
1	0.41 ± 0.19	0.78 ± 0.29	0.26 ± 0.18	0.70 ± 0.32

Table 2

		Non-Preconditioned						Preconditioned					
		$\left(\frac{\Delta\sigma}{\Delta\lambda}\right)_{Cir.}$ (MPa)			$\left(\frac{\Delta\sigma}{\Delta\lambda}\right)_{Rad.}$ (MPa)			$\left(\frac{\Delta\sigma}{\Delta\lambda}\right)_{Cir.}$ (MPa)			$\left(\frac{\Delta\sigma}{\Delta\lambda}\right)_{Rad.}$ (MPa)		
		0.001 s^{-1}	1 s^{-1}	*p*	0.001 s^{-1}	1 s^{-1}	*p*	0.001 s^{-1}	1 s^{-1}	*p*	0.001 s^{-1}	1 s^{-1}	*p*
AV samples at σ = 10 kPa	Sample 1	0.294	2.827	0.0011	0.148	0.940	0.0660	0.727	2.420	0.0206	0.274	0.666	0.0011
	Sample 2	0.439	1.921		0.337	0.251		0.741	0.793		0.210	0.428	
	Sample 3	0.810	2.531		0.068	0.234		0.713	0.718		0.116	0.640	
	Sample 4	1.005	1.524		0.152	0.321		0.667	0.793		0.230	0.335	
	Sample 5	0.356	1.693		0.569	0.813		0.400	0.922		0.154	0.652	
	Sample 6	0.576	1.266		0.284	0.739		0.655	0.672		0.232	0.410	
AV samples at σ = 50 kPa	Sample 1	2.363	4.183	0.0022	0.654	1.805	0.0048	2.353	12.807	0.0206	1.030	5.287	0.0011
	Sample 2	3.175	5.987		0.858	1.1813		2.308	2.804		0.750	2.080	
	Sample 3	2.138	7.708		N/A	0.930		2.285	3.789		0.721	1.867	
	Sample 4	1.764	4.369		N/A	1.276		2.143	4.404		0.832	1.445	
	Sample 5	2.039	3.093		0.546	2.383		3.182	4.422		1.097	2.297	
	Sample 6	1.551	3.742		0.856	2.156		5.365	12.174		1.011	1.359	
AV samples at σ = 100 kPa	Sample 1	3.814	5.839	0.0011	N/A	2.705	N/A	12.144	40.991	0.0206	1.542	5.629	0.0011
	Sample 2	4.172	12.162		N/A	2.488		4.760	7.427		0.774	2.610	
	Sample 3	2.559	14.583		N/A	2.131		4.245	5.397		1.818	2.777	
	Sample 4	2.809	6.024		N/A	1.803		4.008	15.000		1.594	3.469	
	Sample 5	3.689	5.176		N/A	4.061		4.862	5.317		1.852	2.520	
	Sample 6	3.499	5.301		N/A	3.664		5.964	15.484		2.075	2.177	
AV samples at σ = 200 kPa	Sample 1	N/A	7.361	0.0179	N/A	5.604	N/A	20.419	33.735	0.0260	N/A	30.889	N/A
	Sample 2	6.426	9.111		N/A	6.419		8.714	13.087		N/A	6.010	
	Sample 3	3.831	8.225		N/A	4.721		6.371	10.607		2.136	4.244	
	Sample 4	4.252	31.041		N/A	3.415		7.493	19.042		N/A	2.506	
	Sample 5	N/A	34.822		N/A	4.525		N/A	15.305		N/A	N/A	
	Sample 6	N/A	11.328		N/A	4.106		8.260	21.552		1.046	2.664	

Table 3

		Non-Preconditioned						Preconditioned					
		$\left(\frac{\Delta\sigma}{\Delta\lambda}\right)_{Cir.}$ (MPa)			$\left(\frac{\Delta\sigma}{\Delta\lambda}\right)_{Rad.}$ (MPa)			$\left(\frac{\Delta\sigma}{\Delta\lambda}\right)_{Cir.}$ (MPa)			$\left(\frac{\Delta\sigma}{\Delta\lambda}\right)_{Rad.}$ (MPa)		
		0.001 s^{-1}	1 s^{-1}	*p*	0.001 s^{-1}	1 s^{-1}	*p*	0.001 s^{-1}	1 s^{-1}	*p*	0.001 s^{-1}	1 s^{-1}	*p*
PV samples at σ = 10 kPa	Sample 1	0.495	1.352	0.0043	0.151	0.298	0.0022	0.557	0.713	0.0744	0.277	0.409	0.0011
	Sample 2	0.847	1.810		0.129	0.369		0.552	0.686		0.228	0.666	
	Sample 3	0.641	1.557		0.150	0.328		0.656	0.832		0.261	0.314	
	Sample 4	0.331	1.838		0.257	0.359		0.850	1.329		0.197	0.330	
	Sample 5	0.361	0.776		0.326	0.569		0.713	0.753		0.181	0.346	
	Sample 6	0.459	0.698		0.205	0.408		0.564	0.601		0.241	0.563	
PV samples at σ = 050 kPa	Sample 1	2.598	2.489	0.0076	0.678	0.916	0.0011	2.447	2.733	0.0898	0.425	1.519	0.0152
	Sample 2	1.878	2.899		0.379	1.040		3.244	3.482		1.431	1.628	
	Sample 3	1.235	2.849		0.342	0.784		2.688	2.701		0.425	0.858	
	Sample 4	0.739	2.852		0.386	1.112		2.115	3.312		0.684	1.337	
	Sample 5	0.908	1.751		0.714	1.121		1.509	2.626		0.321	0.939	
	Sample 6	1.044	3.370		0.412	0.975		1.182	1.330		0.446	1.235	
PV samples at σ = 100 kPa	Sample 1	3.501	4.554	0.0130	1.194	1.386	0.0022	4.745	7.421	0.0465	1.417	2.181	0.0476
	Sample 2	4.573	6.954		0.585	1.598		10.579	10.857		1.679	1.922	
	Sample 3	3.936	3.556		0.602	1.031		4.237	5.621		N/A	1.544	
	Sample 4	2.864	5.411		0.857	1.490		3.519	5.688		1.300	2.156	
	Sample 5	3.506	7.600		0.881	2.280		3.991	5.464		N/A	2.084	
	Sample 6	2.656	4.391		0.491	1.484		3.054	4.166		N/A	1.527	
PV samples at σ = 200 kPa	Sample 1	5.454	7.013	0.0190	N/A	2.560	N/A	10.457	8.694	0.0465	N/A	3.365	N/A
	Sample 2	5.800	10.231		1.368	5.147		8.644	11.412		N/A	2.633	
	Sample 3	4.406	5.501		N/A	1.338		7.548	8.594		N/A	1.687	
	Sample 4	N/A	7.416		0.857	N/A		6.015	9.496		N/A	2.862	
	Sample 5	N/A	5.483		N/A	3.427		7.018	8.769		N/A	4.717	
	Sample 6	3.339	8.134		N/A	1.567		6.773	8.257		N/A	2.123	

Figure legends

Figure 1 - Intact porcine AV and PV leaflets. The principal loading directions, i.e. the circumferential and radial, are shown in reference to the leaflets. Square specimens (12 × 12mm), shown in scale by dashed lines, were prepared from the central region of the leaflets for in-plane biaxial tests. Insets show a typical histological image of valve cross-section, together with a Maximum Projection Intensity (MPI) representation of the organisation of collagen fibres (collapse of z-stack images) viewed from the fibrosa side of the representative specimens at the central region, up to 45μm depth. Histology was carried out using Alcian Blue/Picro Sirius Red staining, visualising the glycosaminoglycans in blue and collagen fibres in red. The MPI was obtained using second harmonic generation microscopy. While the preferred direction of fibres in both valves is along the circumferential direction, the density of collagen fibre population in PV tissue is visibly less than that of the AV. All scale bars indicate a length of 100μm.

Figure 2 – A representation of the experimental setup: (a) ElectroForce® planar biaxial TestBench, Bose actuators and a custom-designed sample gripping mechanism using BioRake (CellScale®) tines; (b) mounted sample; (c) ink-markers on test specimens; and (d) quadrilaterals reconstructed by tracking those markers in each frame.

Figure 3 - Cauchy stress-stretch ($\sigma - \lambda$) curves for AV and PV samples without preconditioning obtained at (a) $\dot{\lambda} = 1\text{s}^{-1}$ and (b) $\dot{\lambda} = 0.001\text{s}^{-1}$. Curves were constructed by filtering the raw experimental data at each rate $\dot{\lambda}$, using a Savitzky-Golay filter; and (c) averaged data as representative $\sigma - \lambda$ behaviour of all tested samples at each rate. Blue and red colours represent the data in the circumferential and radial directions, and bars present the standard deviation (SD) at each designated point.

Figure 4 - Cauchy stress-stretch ($\sigma - \lambda$) curves for AV and PV samples tested immediately after preconditioning at (a) $\dot{\lambda} = 1\text{s}^{-1}$ and (b) $\dot{\lambda} = 0.001\text{s}^{-1}$. Curves were constructed by filtering the raw experimental data at each rate $\dot{\lambda}$, using a Savitzky-Golay filter; and (c) averaged data as representative $\sigma - \lambda$ behaviour of all tested samples at each rate. Blue and red colours represent the data in circumferential and radial directions, respectively, and bars present the SD at each designated point.

Figure 5 - Two representative filtered $\sigma - \lambda$ curves (using Savitzky-Golay) obtained from tests at $\dot{\lambda} = 1 s^{-1}$ and $\dot{\lambda} = 0.001 s^{-1}$ on the same AV samples, after preconditioning as per the protocol, when stretched for (a) 1mm and (b) 0.75mm. Blue and red colours represent the data in circumferential and radial directions, respectively.

Figure 1

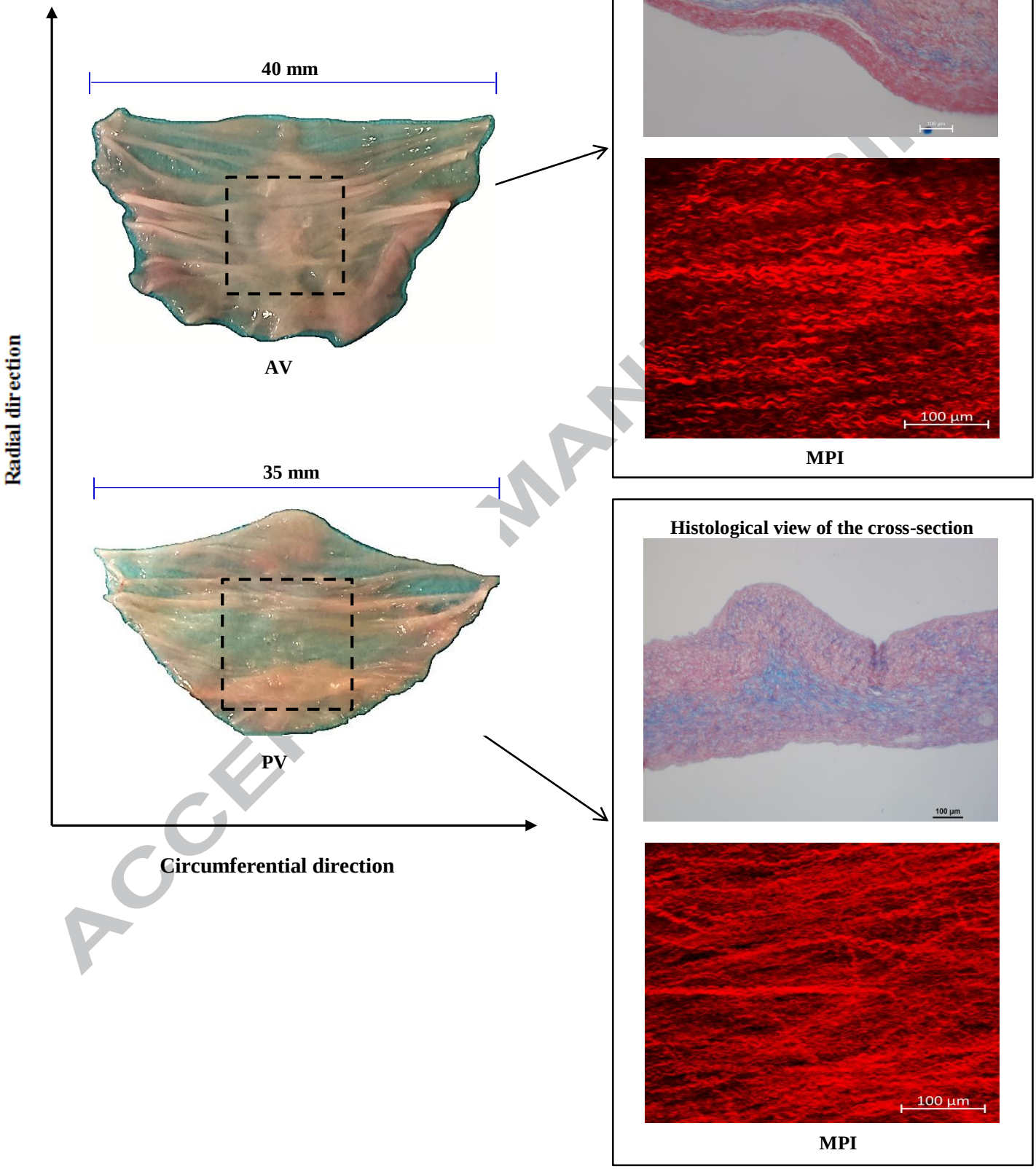

Figure 2

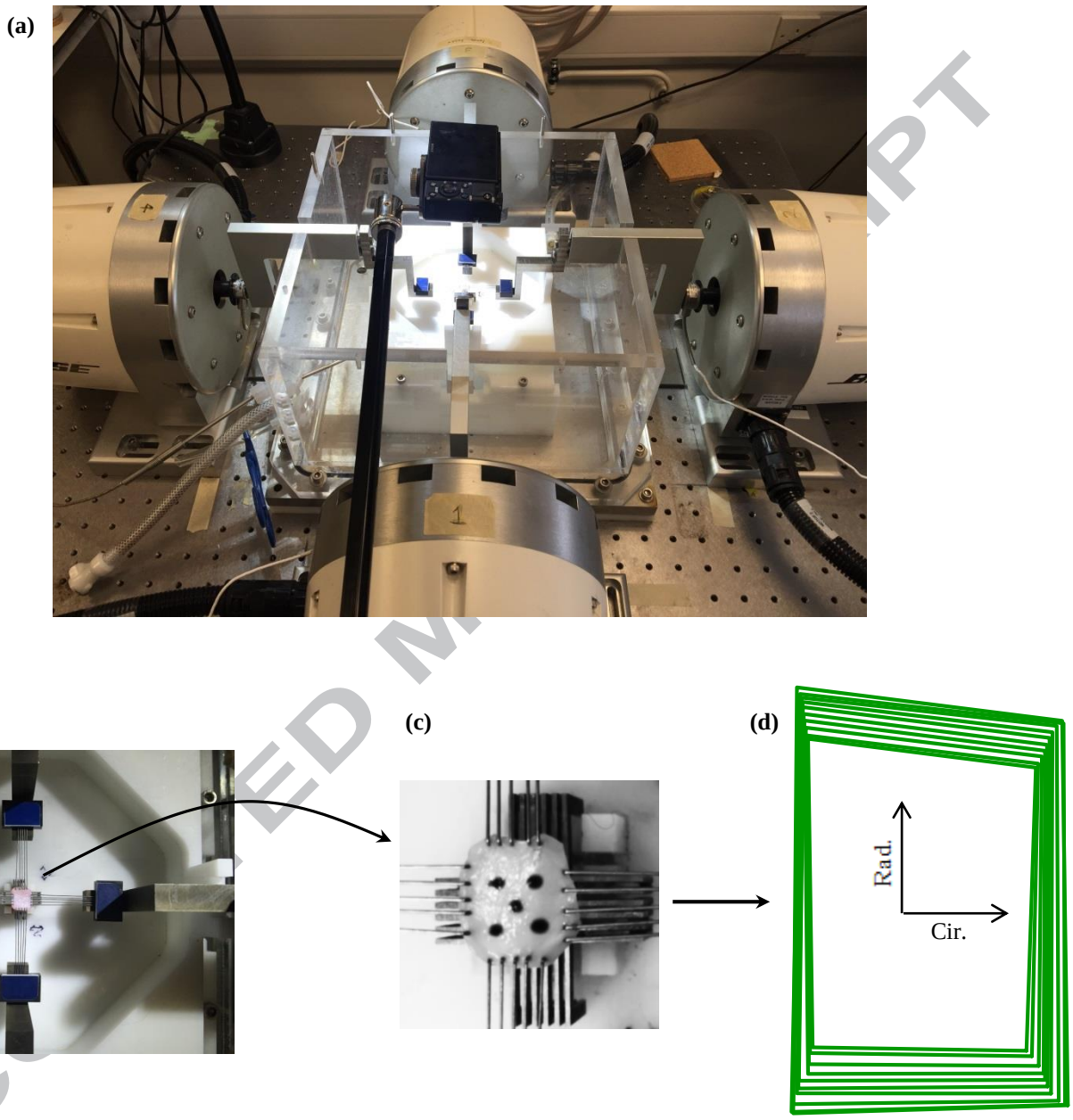

Figure 3

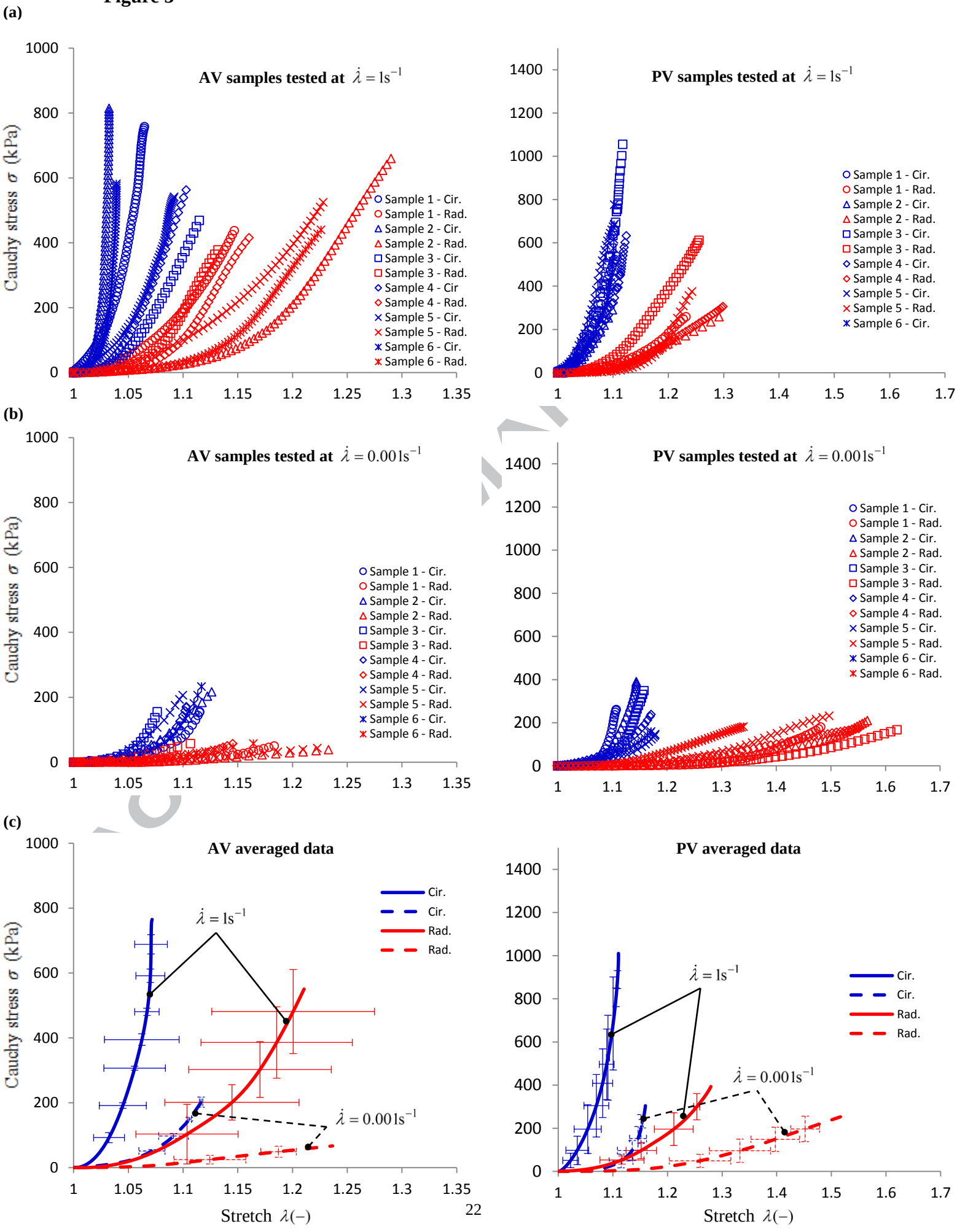

Figure 4

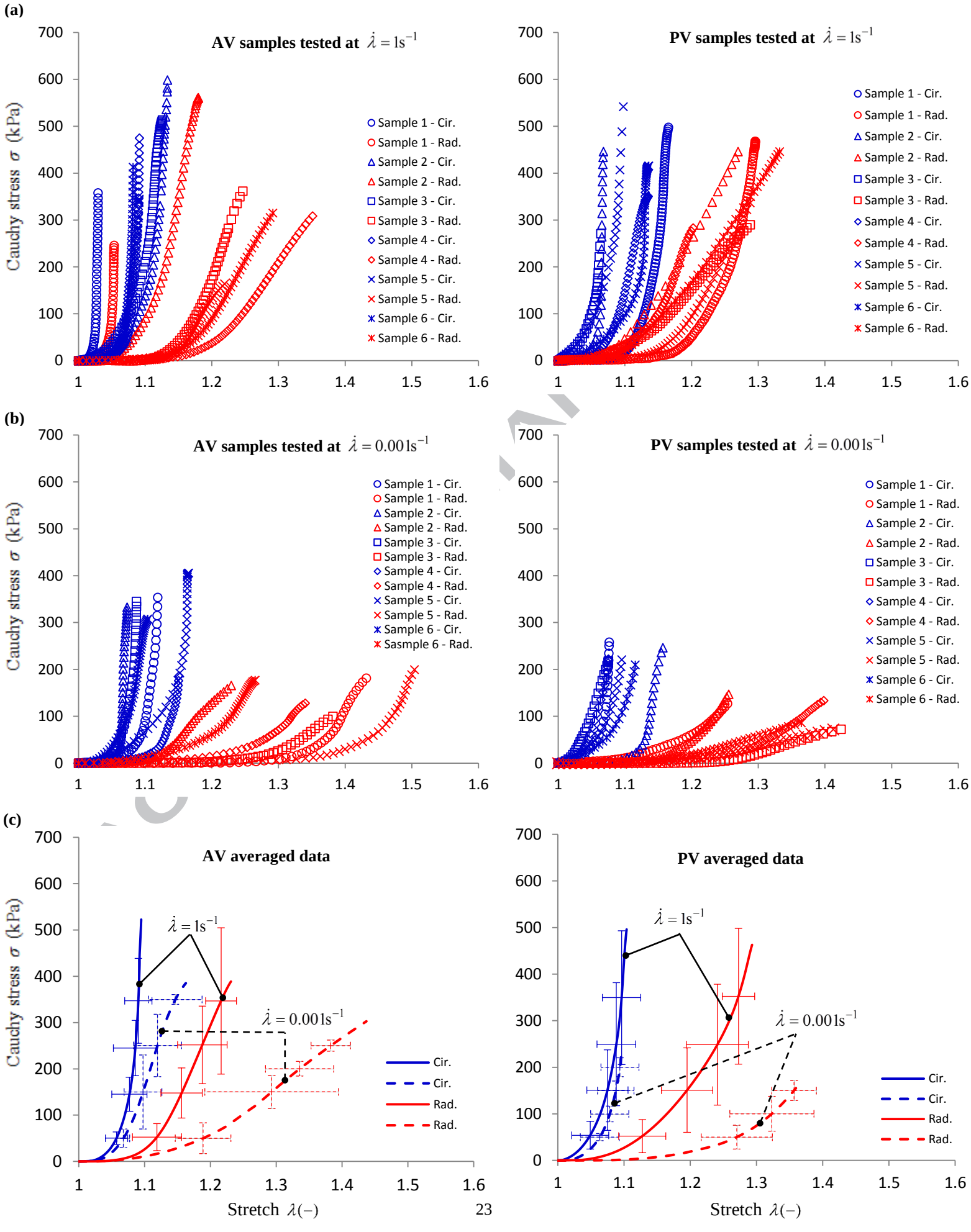

Figure 5

(a)

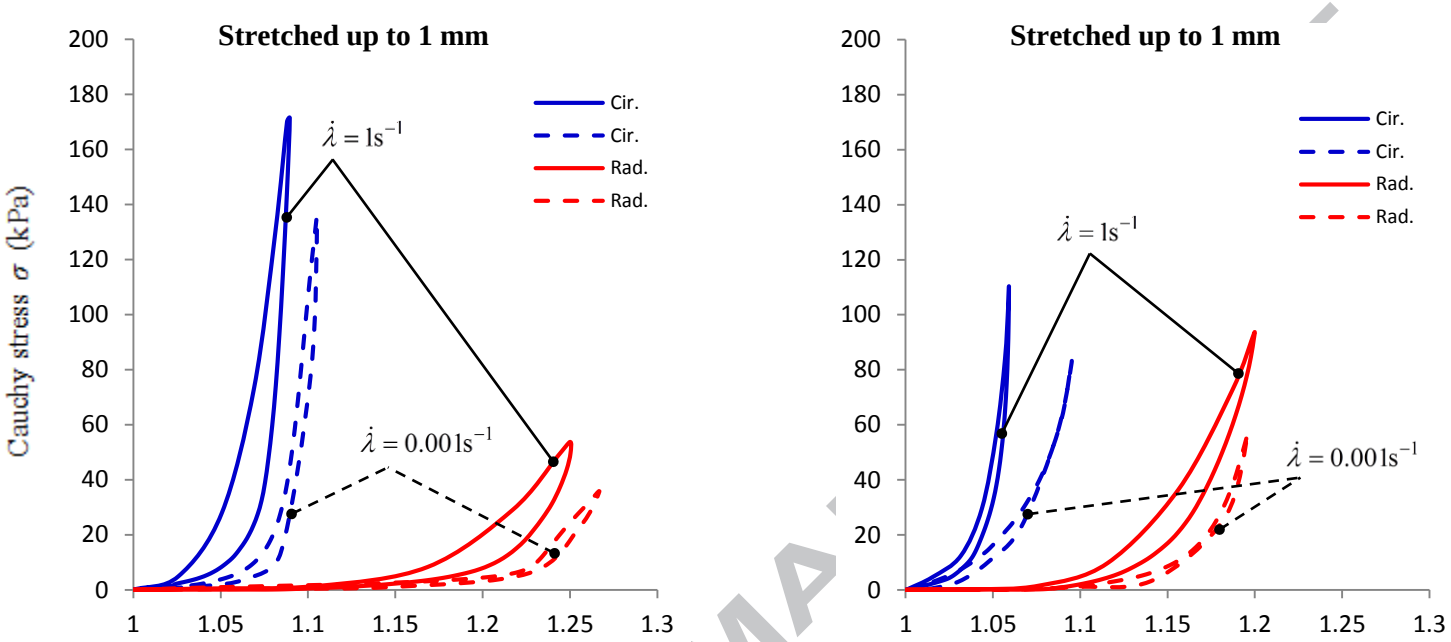

(b)

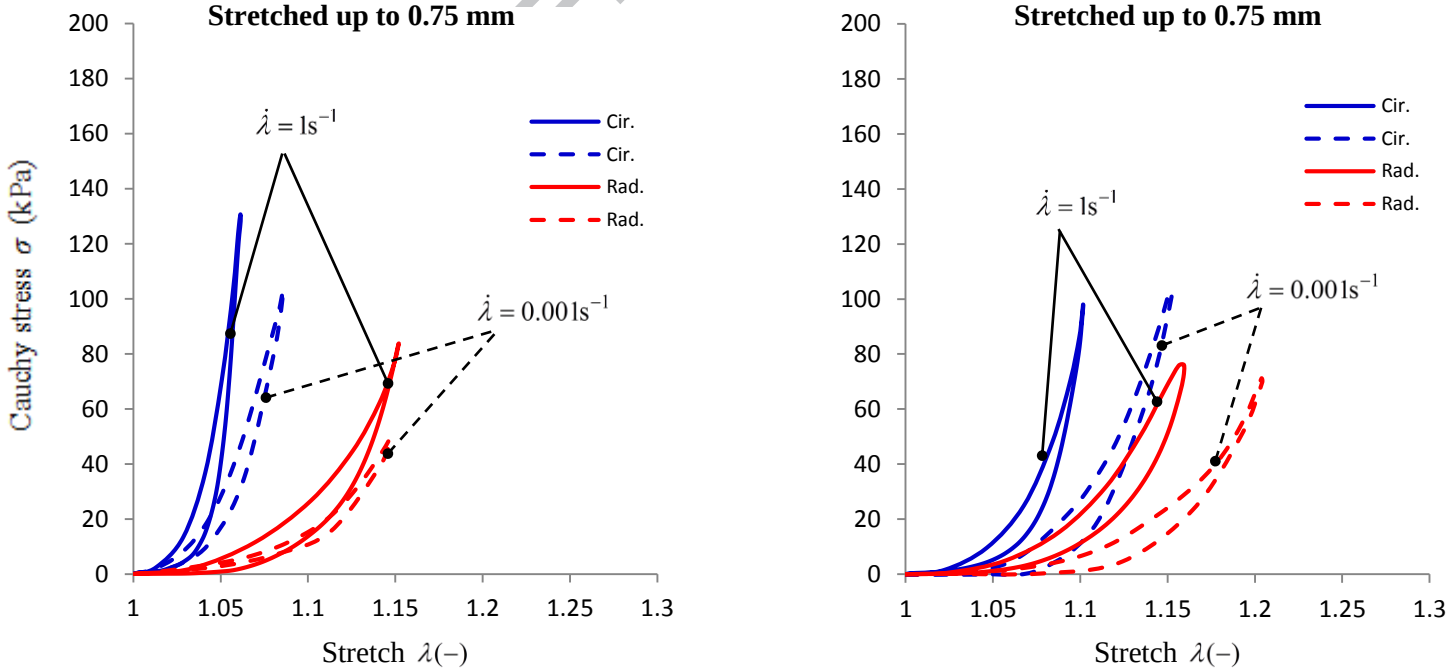

Statement of Significance:

This study presents for the first time a comprehensive set of results and evidence of rate-dependency in the mechanical behaviour of semilunar heart valves under biaxial deformation. Our results challenge the widely-applied assumption in the bulk of the existing literature, where an implicit rate-independency is assumed in both experimental and modelling propositions related to the biomechanics of the aortic and pulmonary valves. This study therefore creates a solid platform for future research in heart valve biomechanics with two important implications. First, experimental campaigns have to be carried out at high stretch rates; ideally as close to the physiological rate as possible. Second, new continuum/computational models are required to address the rate-dependent mechanical behaviour of the semilunar valves.